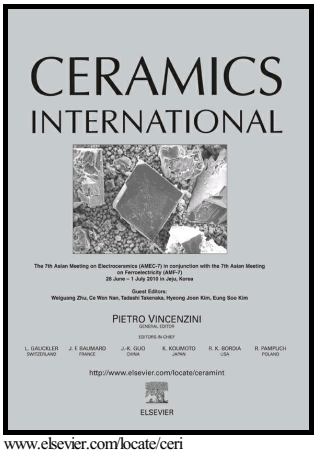

www.elsevier.com/locate/ceri

PRECURSOR SYNTHESIS AND PROPERTIES OF NANODISPERSED TUNGSTEN CARBIDE AND NANOCOMPOSITES WC:nC

Vladimir N. Krasil'nikov, Evgenii V. Polyakov, Nikolai A. Khlebnikov, Nadezda V. Tarakina, Mikhail V. Kuznetsov

PII: S0272-8842(16)32272-6
DOI: http://dx.doi.org/10.1016/j.ceramint.2016.12.026
Reference: CERI14336

To appear in: *Ceramics International*

Cite this article as: Vladimir N. Krasil'nikov, Evgenii V. Polyakov, Nikolai A. Khlebnikov, Nadezda V. Tarakina and Mikhail V. Kuznetsov, PRECURSOR SYNTHESIS AND PROPERTIES OF NANODISPERSED TUNGSTEN CARBIDE AND NANOCOMPOSITES WC:nC, *Ceramics International*, http://dx.doi.org/10.1016/j.ceramint.2016.12.026

PRECURSOR SYNTHESIS AND PROPERTIES OF NANODISPERSED TUNGSTEN CARBIDE AND NANOCOMPOSITES WC:nC

Vladimir N. Krasil'nikov[a], Evgenii V. Polyakov[a], Nikolai A. Khlebnikov[a,b*], Nadezda V. Tarakina[a,c], Mikhail V. Kuznetsov[a]

[a]Institute of Solid State Chemistry, UB RAS, 91 Pervomaiskaya st., Ekaterinburg 620990, Russia

[b]Ural Federal University, 19 Mira st., Ekaterinburg 620002, Russia

[c]Queen Mary University of London, Mile End Road, London E1 4NS, UK

[*]Corresponding author. E-mail: NA.Khlebnikov@urfu.ru, phone: +79126305082.

Abstract

Nanoscale tungsten carbide (WC) and WC:nC nanocomposites have been synthesized by the precursor method. The precursor, obtained in the form of a glassy mass by thermal treatment of a mixture of $(NH_4)_{10}W_{12}O_{41}\cdot 7H_2O$ and glycerol, was heated in inert gaseous atmosphere up to 1050 – 1100 °C. The concentration of chemically active carbon in the precursor and nanocomposites depends on the W/C ratio in the initial mixture. At W/C = 1/3 pure tungsten carbide is formed; at W/C > 1/3 composites of WC and free carbon (WC:nC) are formed. Heating of the precursor with W/C = 1/6 up to 1100 °C in helium atmosphere results in the formation of carbon-encapsulated tungsten carbide nanoparticles. An increase in the precursor-heating rate leads to the formation of chain-like structures. Each chain consists of hexagonal WC grains with unit cell parameters a = 2.93 Å and c = 2.83 Å. Free carbon in WC:nC composites forms agglomerates of carbon "nano-onions" of spherical or multi-layered tubular shapes.

Keywords: carbon, composites, tungsten carbides

1. Introduction

Tungsten carbide (WC) is an important industrial material since it possesses unique physicochemical properties including a high melting temperature, high wear resistance, high resistivity to thermal shock, and a very high hardness close to diamond. Being the hardest among binary carbides, WC is widely applied in the production of abrasive materials and cutting tools [1, 2]. Usually, the presence of pure carbon in WC powders is undesirable, since WC:nC composites have lower hardness [3, 4]. However, nowadays there is a growing interest not only in WC but also in carbon-containing WC:nC composites in the nanostructured form as potential Pt-substituting materials in electrochemical cells used for the electrocatalytic cleaning of waste water and for the production of hydrogen [4-14]. WC:nC nanocomposites loaded with Pt nanoparticles display stronger resistance to CO poisoning and better durability toward methanol electrooxidation compared with the commercial Pt/C catalyst [14, 15]. For application as electrode materials and catalysts, WC and WC:nC need to be produced in the form of nanodispersed powders or aggregates with a highly developed surface. In this respect it is necessary to develop methods for the synthesis of these materials in the nanodispersed state with different morphological and dimensional characteristics of the nanoparticles, as well as in the form of aggregates with high specific surface area.

The traditional carbothermal synthesis method of WC – hours-long solid-state annealing of mixtures of W or WO_3 with carbon at 1400 – 1600 °C in hydrogen atmosphere – is widely used for the production of high-purity crystalline tungsten

carbide [2]. This approach is very energy-consuming, and it cannot be applied for obtaining nanodispersed samples due to the recrystallization phenomenon. Among the methods for the synthesis of WC and WC:nC nanoscale powders described in the literature, the precursor synthesis based on different colloidal precursors of tungsten and carbon is very promising [16-28]. There are several variations of the precursor method for the synthesis of nanodispersed tungsten carbide, differing in the choice of initial reagents: tungstic acid (H_2WO_4) or ammonium tungstates (for example $(NH_4)_2WO_4$, $(NH_4)_{10}W_{12}O_{41}\cdot 5H_2O$ or $(NH_4)_6H_2W_{12}O_{40}\cdot xH_2O$) are used as a source of tungsten and organic compounds, and polymers (such as citric acid, n-octylamine, resorcinol, polyacrylonitrile, polyaniline and carbohydrates) are used as a source of carbon. The reagents are mixed in water or organic solvent, and then the obtained mass is dried. The obtained precursor is treated thermally in inert gaseous medium or in vacuum. This method allows the synthesis temperature to be decreased to 1000 – 1100 °C. Another approach relies on the use of tungsten carbonyl $W(CO)_6$ as a precursor, the vapors of which are decomposed at 600 – 800 °C accompanied by the formation of WC nanopowder [27]. Its advantages include the possibility of mixing components at the molecular level, controlling precursor and product particle dispersion, low synthesis temperature, as well as a short synthesis time compared to the traditional carbothermal method. The formation of excessive free carbon during thermolysis of the organic component is usually considered as a drawback of the precursor methods; to remove excessive free carbon, products of thermolysis are calcinated in a mixture of argon and hydrogen [25]. However, for applications as components in electrochemical cells, the presence of carbon is an advantage, especially if during the synthesis the morphology of both WC nanoparticles and carbon support can be controlled. Thus, detailed knowledge

of the physicochemical conditions of formation as well as of the properties of the excessive free carbon, which usually accompanies carbides in the synthesis, is of great importance [17, 18] and would allow the synthesis of nanodispersed carbonless WC or WC:nC materials with specific properties and for particular applications. Consequently, the aim of this study is to understand chemical, phase, and morphological changes that occur during the thermally stimulated transformations of initially molecular-dispersed metal-organic precursors and to develop the precursor-based approach, which allows to control the excess and the morphology of free carbon in WC:nC nanocomposites.

2. Experimental

Nanodispersed WC and WC:nC were synthesized using $(NH_4)_{10}W_{12}O_{41}\cdot 7H_2O$ and glycerol ($C_3H_8O_3$) as tungsten and carbon sources, respectively. The ratios of the reagents $(NH_4)_{10}W_{12}O_{41}\cdot 7H_2O$ (99.9%) and $C_3H_8O_3$ (99.9%) required for the production of tungsten carbide containing no impurity carbon were taken in accordance with the following reaction [17]:

$$(NH_4)_{10}W_{12}O_{41}\cdot 7H_2O + 12C_3H_8O_3 = 12WC + 24CO + 10NH_3 + 60H_2O \quad (1)$$

Equation (1) represents a summary reaction, which does not show the full complexity of the chemical process. For the production of WC:nC nanocomposites, the concentration of glycerol was increased. The initial substances were thoroughly mixed in heat-resistant glass beakers and heated on a hot plate at 100 – 150 °C until the $(NH_4)_{10}W_{12}O_{41}\cdot 7H_2O$ crystals were completely dissolved in glycerol and a transparent colorless gel was formed. The process of gel formation was accompanied by the evaporation of water and ammonia; increasing the temperature to 220 – 250 °C speeds up this evaporation, upon completing of which the gel has hardened and turned into a

black glassy mass having a composition close to the hypothetical compound $WO_2(C_3H_6O_3)$ [17] (Figure 1 a, b). The material produced in this way was ground in a porcelain mortar and then, as a precursor, heated stepwise in helium atmosphere at 400 – 1100 °C.

Phase analysis was carried out using a POLAM S-112 polarized-light microscope in transmission mode and a STADI-P X-ray diffractometer (STOE, Germany) using Cu-Kα radiation in the 2θ range 10° to 60° with a step of 0.02°. The obtained X-ray powder diffraction patterns were compared with those in the Powder Diffraction File – PDF2 database (ICDD, USA, release 2009). The Debye-Scherrer method was used to determine the size of the particles from the X-ray diffraction patterns. The microstructure of the particles were studied by means of scanning (SEM) and transmission (TEM) electron microscopy using JSM JEOL 6390LA and FEI Titan 80-300 microscopes, respectively. Raman spectra of the powders were collected with a RENISHAW-1000 spectrometer (λ = 514.5 nm, Ar^+-laser). The specific surface area was estimated by means of the BET low-temperature nitrogen sorption method with a TriStar 3000 auto analyzer. The carbon content in the samples was determined by a tried-and-true method on a METABAK-CS-10 gas analyzer [17]. The electronic state of the surface of the synthesis products was analyzed by X-ray photoelectron spectroscopy (XPS) methods using an ESCALAB MK II electron spectrometer with nonmonochromatic Mg-K_α radiation (1253.6 eV).

3. Results and discussion

3.1. X-ray powder diffraction and scanning electron microscopy

Microscopic analysis of the precursor samples produced by thermal treatment of organometallic solutions and gels with the $(NH_4)_{10}W_{12}O_{41}\cdot 7H_2O/C_3H_8O_3$ ratio equal to 1/12 (designated as "I"), 1/16 ("II"), and 1/20 ("III") at 220 – 250 °C, revealed that all of them are glassy optically isotropic substances of dark-grey or black colour depending on the temperature and duration of calcination. The black colour of the precursor is due to the presence of elementary carbon formed as a result of thermal transformations of the organic component of the gel. Most of the precursor dissolves in hot water during mixing, while carbon contained in the precursor precipitates as a black sediment.

The SEM images shown in Fig. 1 demonstrate the change in the morphology of the samples produced by heating of precursors at 200, 240, 500, 600, 800, and 1100 °C in helium atmosphere. Reaction temperatures were carefully chosen based on the observed properties of the reaction products after each stage of the thermal treatment and in accordance with available literature data about phase transformations in related systems [22-28].

Changes in the composition and morphology of powders with annealing temperature are summarized in Table 1. The products of annealing the precursor at 400 °C are amorphous according to X-ray data (Fig. 2), which agrees with the absence of phase contrast in the optical microscope. Poorly resolved lines of the oxide $W_{18}O_{49}$ appear on the X-ray diffraction patterns of the samples heated at 600 – 750 °C [29, 30]; the lines of WO_2, W, W_2C, and WC emerge after annealing of the precursor at 800, 850, 950, and 1000 °C, respectively (Fig. 2). The lines of tungsten carbide oxide $W_{18}O_{49}$ on the X-ray diffraction pattern (Fig. 2) correspond to the wire-like crystals seen in Fig. 1 (e, f). Particles of W, W_2C and WC have a granular structure. The concentration of free carbon after annealing of the precursor (I) at 1100 °C for 10 min was found to be 0.26

wt% and the X-ray diffraction pattern showed the formation of hexagonal tungsten carbide, WC (Fig. 2).

Based on the X-ray diffraction data and elemental analysis data, the sequence of solid phase transformations upon heating of the precursors (I) in the temperature interval 400 – 1100 °C in helium atmosphere can be described as follows Eq. 2:

$$WO_2(C_3H_6O_3) \rightarrow X \rightarrow W_{18}O_{49} \rightarrow WO_2 \rightarrow W \rightarrow W_2C \rightarrow WC \qquad (2)$$

where X stands for the X-ray amorphous phase. Each phase in this sequence is formed through the interaction of the previous phase with carbon as the temperature increases. A similar scheme of phase transformations was proposed [26] to describe the interaction of WO_3 with carbon obtained by heat treatment of the gel formed by $(NH_4)_6H_2W_{12}O_{40}{\cdot}nH_2O$ and glucose and for a description of the thermolysis of the $(C_8H_{17}NH_3)_2WO_4$ precursor isolated from non-aqueous medium [22].

On the X-ray diffraction pattern of the sample produced by thermal treatment of precursor (II), in addition to the lines from hexagonal WC, a line at d = 4.6189 Å and a diffuse halo in the 2θ range 18 – 25° were observed (Fig. 2). These features are caused by the presence of structured and amorphous carbon [11]. Since the concentration of carbon in the precursor depends on the amount of glycerol in the initial reaction mixture, this method allows one to synthesize WC:nC composites containing different amounts of free carbon. So, because of heating of precursors (II) and (III) in helium atmosphere, WC:nC composites are formed, containing 11.2 and 18.6 wt% free carbon, respectively. Excess of organic reagent in the precursor does not change the above-described sequence of phase formations, but affects the process of WC:nC composite formation: for its completion it is sufficient to heat precursor (II) up to 1100 °C and precursor (III) up to 1000 – 1050 °C with a rate of 15 °/min. Homogeneous tungsten

carbide can be produced by thermal treatment of a precursor having a composition similar to that of the hypothetical compound $WO_2(C_3H_6O_3)$. In the absence of glycerol, the thermal transformation of $(NH_4)_{10}W_{12}O_{41}\cdot 7H_2O$ in helium atmosphere leads to the formation of a dark blue powder of $W_{18}O_{49}$.

For all three precursors, the described carbothermal transformations occur at relatively high rate and low temperatures, allowing obtaining tungsten oxides and then tungsten carbides in the form of nanoparticles. The nano-sized dimensions of WC and WC:nC composites were confirmed by electron microscopy (Figs. 1, 3, 4). The WC:nC composite obtained by heating precursor (II) up to 1000 °C in helium atmosphere can be described by tungsten carbide nanoparticles distributed in a carbon cellular matrix (Table 1). If the heating rate is doubled, in addition to nanoparticles (10 – 60 nm in size) "frame structures" are formed, which consist of chains of WC grains oriented at 60° with respect to each other (Fig. 3 a – d). The electron diffraction patterns obtained from these structures can be indexed in a hexagonal cell with parameters a = 2.93 Å and c = 2.83 Å. Tungsten carbide grains in the chains contain a large amount of stacking faults alternating along the a axis of the crystal. Most of the observed defects can be described by the displacement vector 1/6 <1 1 -2 3> in the {1 -1 0 0} planes typical of the hexagonal structure of WC (Fig. 3 e, f). The carbon observed in the sample forms agglomerates consisting of graphitic carbon, multi-layered "onion structures" [31] with a spherical shape or the shape of multi-walled nanotubes (Fig. 4).

In order to separate free carbon from composite powders obtained after annealing of precursors (II) and (III) (free carbon content in these samples was 11.2 wt% 18.6 wt%, respectively) we used a hot solution of concentrated hydrofluoric acid with a small addition of nitric acid. These acids dissolve the tungsten carbide phase

completely. Alternatively, composites can be treated with formic acid [32, 33]. The resulting black bulky mass of free carbon was vacuum-filtered from the solution, washed with distilled water, and dried at 200 °C in air for 1 h. The specific surface areas of carbon samples (II) and (III) determined from the low-temperature nitrogen adsorption data, were 1128 and 1200 m^2/g, respectively. The cellular morphology of the carbon residual mass removed from WC:nC composite powder (III) reflects the structure of the colloidal state of the precursor formed during high-temperature decomposition of the colloidal solution at 200-250 °C, Fig. 5.

3.2. Raman spectroscopy

The Raman spectra of the of precursor (I) and products of its annealing in helium atmosphere in the temperature range 400 - 600 °C contain intensive lines at 1364 and 1597 cm^{-1} (Fig. 6) typical of free carbon [34, 35]. The line at 1338 cm^{-1} (D-line) is due to vibrations of the C–C bonds in the sp^3-hybrid state. Considerable broadening and high intensity of the D-line suggests the presence of small ordered regions of graphitic carbon, which is corroborated by the position and the intensity of the line at 1599 cm^{-1} (G-line) [36-38]. The line at 2000 cm^{-1} has been attributed to the C–O vibrational modes of oxidized graphene [39-41]. An increase of the annealing temperature up to 600 °C makes the line at 2000 cm^{-1} more pronounced. A broad diffuse line in the 2300 - 3300 cm^{-1} region is associated with the C–H bond vibrations and D- and G-mode vibrations of the graphitic-carbon planes in free carbon [37-38]. The observed Raman spectra are similar to those of WO_3/GO composites (GO stands for graphene oxide) [39]. In the low-frequency region of the spectra, narrow well-resolved lines at 803, 704, 262, and 127 cm^{-1} are observed, which are typical of the O–W–O

bond vibrations in the structure of WO_3, WO_2, and $W_{18}O_{49}$ oxides [29, 30, 42]. The Raman spectrum of the sample produced by annealing precursor (III) at 1100 °C in helium atmosphere also features all characteristics of the vibrational spectra of free carbon having the form of oxidized graphitic carbon: two rather intense lines at 1343 cm^{-1} (D-line) and 1592 cm^{-1} (G-line) are observed together with the lines of the vibrational spectrum of the basic WC phase (Fig. 7). After removal of the WC phase from the WC:nC nanocomposite by acid treatment, the Raman spectrum of the carbon sample features only carbon lines, which we assigned to oxidized graphitic carbon (nano-onions and tubular structures): narrow intense lines of approximately the same intensity at 1344 and 1594 cm^{-1}, broad central lines at 2688 and 2920 cm^{-1} and a weak line at ~3180 cm^{-1}, which are composite lines (overtones) since they can be obtained from doubling of the D- and G-line, respectively, or by their combined addition [43] (Fig. 7).

3.3. X-ray photoelectron spectroscopy

The XPES measurements allowed us to obtain additional information about the oxidation state of tungsten and the chemical forms of carbon (and oxygen) in the powders of carbon-containing composites WC:nC. By combining Ar^+ ion beam etching of the sample surface and energy analysis of photoelectrons, we also quantitatively estimated the average content of W, C, and O in different chemical forms on the surface of WC:nC particles and at varying depths. The spectra were analyzed taking into account that during ion etching the light atoms (C and O) could be removed from the surface much easier than tungsten. As a result, the reduction of oxides and carbides, which present on the particle surface, is probable. The overview XPE spectrum of the

WC:nC powder containing 18 wt% carbon (Fig. 8) recorded before argon ion etching exhibits intense W4*f*, C1*s*, and O1*s* lines. The spectra of these internal electronic states both for the surface and after three ion-sputtering events (1, 4, and 14 min) are shown in Fig. 8.

The W4*f* band consists of two doublets corresponding to the $4f_{7/2}$ and $4f_{5/2}$ lines of tungsten (Fig. 8), which are attributed to tungsten carbide WC and oxide WO_3. In practice it is difficult to distinguish between the WC phase and metallic tungsten from an analysis of W4*f* lines only. The formation of the WC phase is confirmed by the presence of a component of the C-W bond in the energy spectrum of the C1s level. A quantitative estimation of the ratio of carbon atoms in C-W form and tungsten atoms in W-C form (see the bar graph in Fig. 9) points towards carbon deficiency at the surface of WC particles. Therefore, WC, W_2C, and metallic tungsten phases can be expected to be present in the powder. As mentioned above, besides tungsten carbide, the W4*f* band contains a doublet attributed to WO_3. WO_3 is present on the surface and is gradually removed as the powder is polished with the ion beam. As a result of ion bombardment, the tungsten band originating from WC broadens first due to destruction of the carbide structure by the ion beam, and second due to partial reduction of WC to WC_x (x = 0.9 – 1) or to W_2C. The main chemical components of the WC:nC powder and the semi-quantitative tendency of the change in their average content measured from the surface into the bulk of the particles are shown in Fig. 9.

As ion cleaning of the surface of WC:nC particles proceeds, the line associated with the C-C bond at 284.05 eV begins to dominate in the C1s band (Fig. 8). This line is a signature of graphite- and diamond-like forms of carbon, amorphized graphene, carbon nanotubes, fullerenes, and graphene films [44]. The second component in the

C1s band is attributed to carbide states of carbon in WC or in WC_x. Finally, in the region of high binding energies, there are components that we ascribe to organic forms of carbon adsorbed on the surface during storage of the powders in air. During ion etching, the intensity of the C-C band decreases and that of the C-W band increases, indicating that tungsten carbide localizes in the core of the particles, whereas the phases with C-C bonds dominate at the surface (free carbon, presumably in the form of thin molecular layers of oxidized graphene). The ratio between these two forms of carbon varies from 7:1 to 3:1 when going from the surface into the bulk of the composite particles. Lines from tungsten oxide WO_3 and oxygen bound with carbon can be distinguished on the oxygen spectra (Fig. 8). The latter can be related both to organic contaminations on the surface and to oxidized graphene. Tungsten oxide WO_3, which is likely to be the product of oxidation of a WC nanoparticle's surface by atmospheric oxygen, is removed from the surface by ion etching.

4. Conclusions

The proposed method, based on the heating of organic-inorganic $(NH_4)_{10}W_{12}O_{41}\cdot 7H_2O/C_3H_8O_3$ homogeneous gel-like precursors, enables, by varying the amount of chemically active carbon in the precursor, obtaining both single-phase WC and WC:nC composites with tungsten carbide particles of nanometre size (5-60 nm). The carbothermal reduction of the precursor to carbide can proceed through different stages, depending on the initial composition of the precursor. For the formation of WC:nC nanocomposite and nanodispersed WC containing 99.9 wt% of the main product, it is sufficient to heat the precursors with a preset W:C ratio up to a maximal temperature of 1100 °C. At 1000 – 1100 °C this transformation takes place within 10-20

min, which is very fast for carbothermal synthesis, suggesting that the process of reduction is under kinetic control. The reason why our carbothermal reduction is kinetically controlled may lie in the self-organization of the precursor as the colloid, which is similar to nematic liquid crystals [16]. The most important feature of the proposed precursor method for the synthesis of WC or WC:nC nanocomposites is, in our opinion, the combination of the following factors: (1) preparation of the precursor in the form of a non-aqueous liquid solution of an organometallic compound that is homogeneous at low temperatures; (2) transformation of the homogeneous solution into a gel and then into a glassy state through heating; (3) the use of a liquid chemical reagent (glycerol) as a carbon source for carbothermal reduction of tungsten and formation of WC. Free carbon separated from the WC:nC composites inherited cellular morphology and thereof showed high values of specific surface area (1200 m^2/g).

Acknowledgment

This work was supported by Act 211 Government of the Russian Federation, agreement No. 02.A03.21.0006.

References

[1] W. Liu, Y. Soneda, H. Haton, A novel carbothermal method for the preparation of nano-sized WC on high surface area carbon, Chem. Lett. 35 (2006) 1148–1149.

[2] Z.Z. Fang, X. Wang, T. Ryu, K.S. Hwang, H.Y. Sohn, Synthesis, sintering, and mechanical properties of nanocrystalline cemented tungsten carbide – A review, Int. J. Refract. Met. Hard Mater. 27 (2009) 288–299.

[3] C. Liu, D. Zhou, J. Zhou, Z. Xie, Y. Xia, Synthesis and characterization of tungsten carbide and application to electrocatalytic hydrogen evolution, RSC Adv. 6 (2016) 76307–76311.

[4] T. Ryu, H.Y. Sohn, K. S. Hwang, Z. Z. Fang, Tungsten carbide nanopowder by plasma-assisted chemical vapour synthesis from WCl_6-CH_4-H_2 mixtures, J Mater Sci, 43 (2008) 5185–5192.

[5] M. Rosenbaum, F. Zhao, M. Quaas, H. Wulff, U. Schorder, F. Scholz, Evaluation of catalytic properties of tungsten carbide for the anode of microbial fuel cells, Appl. Catal., B 74 (2007) 262–270.

[6] M. Eriksson, M. Radwan, Z. Shen, Spark plasma sintering of WC, cemented carbide and functional graded materials, Int. J. Refract. Met. Hard Mater. 36 (2009) 31–37.

[7] F. Harnisch, G. Sievers, U. Schroder, Tungsten carbide as electrocatalyst for the hydrogen evolution reaction in pH neutral electrolyte solutions, Appl. Catal., B 89 (2009) 455–458.

[8] S. Aravinth, B. Sankar, M. Kamaraj, S.R. Chakravarthy, R. Sarathi, Synthesis and characterization of hexagonal nano tungsten carbide powder using multi walled carbon nanotubes, Int. J. Refract. Met. Hard Mater. 33 (2012) 53–57.

[9] C.K. Poh, S.H. Lim, Z. Tian, L. Lai, Y.P. Feng, Z. Shen, J. Lin, Pt-W_xC nano-composites as an efficient electrochemical catalyst for oxygen reduction reaction, Nano Energy 2 (2013) 28–39.

[10] Y. Mateyshina, A. Ulihin, A. Samarov, C. Barnakov, N. Uvarov, Nanoporous carbon-based electrode materials for supercapacitors, Solid State Ionics 251 (2013) 59–61.

[11] G. Singla, K. Singh, O.P. Pandey, Structural and thermal analysis of in situ synthesized C–WC nanocomposites, Ceram. Int. 40 (2014) 5157–5164.

[12] A.L. Tomas-Garcia, Q. Li, J.O. Jensen, N.J. Bjerrum, High Surface Area Tungsten Carbides: Synthesis, Characterization and Catalytic Activity towards the Hydrogen Evolution Reaction in Phosphoric Acid at Elevated Temperatures, Int. J. Electrochem. Sci. 9 (2014) 1016–1032.

[13] G. Singla, K. Singh, O.P. Pandey, Synthesis of carbon coated tungsten carbide nano powder using hexane as carbon source and its structural, thermal and electrocatalytic properties, Int. J. Hydrogen Energy 40 (2015) 5628–5637.

[14] L. Xiong, L. Zheng, C. Liu, L. Jin, Q. Liu, J. Xu, Tungsten Carbide Microspheres with High Surface Area as Platinum Catalyst Supports for Enhanced Electrocatalytic Activity, J. Electrochem. Soc. 162 (2015) F468–F473.

[15] L. Jiang, H. Fu, L. Wang, G. Mu, B. Jiang, W. Zhou, R. Wang, Tungsten carbide/porous carbon composite as superior support for platinum catalyst toward methanol electro-oxidation, Mat. Res. Bul., 49 (2014) 480-486

[16] E.V. Polyakov, L.G. Maksimova, V.N. Krasilnikov, V.A. Zhilyaev, T.A. Timoshchuk, O.N. Ermakova, G.P. Shveikin, I.V. Nikolaenko, Thermally stimulated transformation of micellar structure of tungsten glycolate into nanodispersed tungsten carbide [in Russian], Doklady AN 434 (2010) 200–203.

[17] E.V. Polyakov, V.N. Krasilnikov, A.P. Tyutyunnik, N.A. Khlebnikov, G.P. Shveikin, Precursor synthesis of nanodispersed tungsten carbide WC and nanocomposites WC:nC [in Russian], Doklady AN 457, 2 (2014) 189–192.

[18] N.A. Khlebnikov, E.V. Polyakov, S.V. Borisov, O.P. Shepatkovskii, V.N. Krasil'nikov, Application of Nanocomposite Track Membranes for Electron Microscopy Samples Preparation, Advanced Materials Research 1082 (2015) 51–56.

[19] H. Preiss, B. Meyer, C. Olschewski, Preparation of molybdenum and tungsten carbides from solution derived precursors, J. Mater. Sci. 33 (1998) 713–722.

[20] R. Koc, S.R. Kodambaka, Tungsten carbide (WC) synthesis from novel precursors, J. Eur. Ceram. Soc. 20 (2000) 1859–1869.

[21] J.C. Kim, B.K. Kim, Synthesis of nanosized tungsten carbide powder by the chemical vapor condensation process, Scripta Mater. 50 (2004) 969–972.

[22] M.F. Zawrah, Synthesis and characterization of WC-Co nanocomposites by novel method, Ceram. Int. 33 (2007) 155–161.

[23] Y. Yamashita, T. Harada, T. Makino, K. Fujiyoshi, S. Ueno, M. Koga, Fabrication of high purity and nano-sized tungsten carbide particles using chemical complex solution, J. Jpn. Soc. Powder. Powder Metallurgy 57 (2009) 348–351.

[24] D. Chen, H. Wen, H. Zhai, H. Wang, X. Li, R. Zhang, J. Sun, L. Gao, Novel synthesis of hierarchical tungsten carbide micro-/nanocrystals from a single-source precursor, J. Am. Ceram. Soc. 93 (2010) 3997–4000.

[25] K.M. Reddy, T.N. Rao, J. Joardar, Stability of nanostructured W-C phases during carburization of WO_3, Mater. Chem. Phys. 128 (2011) 121–126.

[26] Y. Jin, D. Liu, X. Li, R. Yang, Synthesis of WC nanopowders from novel precursors, Int. J. Refract. Met. Hard Mater. 29 (2011) 372–375.

[27] Y. Jin, X. Li, D. Liu, C. Liu, R. Yang, Phase and microstructure evolution during the synthesis of WC nanopowders via thermal processing of the precursor, Powder Technol. 217 (2012) 482–485.

[28] N.M. Gavrilov, I.A. Pasti, J. Krstic, M. Mitric, G. Ciric-Marjanovic, S. Mentus, The synthesis of single phase WC nanoparticles/C composite by solid state reaction involving nitrogen-rich carbonized polyaniline, Ceram. Int. 39 (2013) 8761–8765.

[29] D.Y. Lu, I.J. Chen, J. Zhou, S.Z. Deng, N.S. Xu, J.B. Xu, Raman spectroscopic study of oxidation and phase transition in $W_{18}O_{49}$ nanowires, J. Raman Spectrosc. 38 (2007) 176–180.

[30] S. Jeon, K. Yong, A novel composite hierarchical hollow structure: one-pot synthesis and magnetic properties of $W_{18}O_{49}$–WO_2 hollow nanourchins, Chem. Commun. 45 (2009) 7042–7044.

[31] F.C.B. Maia, R.E. Samad, J. Bettini, R.O. Freitas, N.D. Vieira Junior, N.M. Souza-Neto, Synthesis of diamond-like phase from graphite by ultrafast laser driven dynamical compression, Scientific Reports 5 (2015) 11812.

[32] O.I. Gyrdasova, V.N. Krasil'nikov, E.V. Shalaeva, I.V Baklanova., M.A. Melkozerova, L.Y. Buldakova, M.Y. Yanchenko, Optical and photocatalytic properties of quasi-one-dimensional ZnO activated by carbon, Mendeleev Commun. 24 (2014) 143–144.

[33] E.V. Shalaeva, O.I. Gyrdasova, V.N. Krasil'nikov, M.A. Melkozerova, I.V. Baklanova, L.Y. Buldakova, Structural, optical and photocatalytic properties of quasi-one-dimensional nanocrystalline ZnO, ZnOC:nC composites and C-doped ZnO, Nanocomposites, Nanophotonics, Nanobiotechnology, and Applications. Series: Springer Proceedings in Physics 156 (2015) 313–336.

[34] S. Osswald, Y. Gogotsi, In Situ Raman Spectroscopy of Oxidation of Carbon Nanomaterials, Raman Spectroscopy for Nanomaterials Characterization (2012) 291–351.

[35] C. Zhang, M. Lv, X. Wang, J. Li, X. Yang, J. Yang, H. Hu, Controllable synthesis and formation mechanism of carbon micro/nano-structural materials, Chem. Phys. Lett. 586 (2013) 121–126.

[36] S. Reich, C. Thomsen, Raman spectroscopy of graphite, Phil. Trans. R. Soc. Lond. A. 362 (2004) 2271–2288.

[37] P.K. Chu, L. Li, Characterization of amorphous and nanocrystalline carbon films, Mater. Chem. Phys. 96 (2006) 253–277.

[38] M.A. Pimenta, G. Dresselhaus, M.S. Dresselhaus, L.G. Canceado, A. Jorio, R. Saito Studying disorder in graphite-based systems by Raman spectroscopy, Phys. Chem. Chem. Phys. 9 (2007) 1276–1291.

[39] Y. Gui, J. Yuan, W. Wang, J. Zhao, J. Tian, B. Xie, Facile Solvothermal Synthesis and Gas Sensitivity of Graphene/WO_3 Nanocomposites, Materials 7 (2014) 4587-4600.

[40] M. Passoni, V. Russo, D. Dellasega, F. Causa, F. Ghezzi, D. Wolverson, C.E. Bottani, Raman spectroscopy of nonstacked graphene flakes produced by plasma microjet deposition, J. Raman Spectrosc. 43 (2012) 884–888.

[41] J.E. Flores-Mena, J. Diaz-Reyes, J.A. Balderas-Lopez, Structural properties of WO_3 dependent of the annealing temperature deposited by hot-filament metal oxide deposition, Revista Mexicana de Fisica 58 (2012) 504–509.

[42] H.S. Wahab, S.H. Ali, A.M. Abdul Hussein, Synthesis and Characterization of Graphene by Raman Spectroscopy, Journal of Materials Sciences and Applications 1 (2015) 130-135.

[43] M.A. Pimenta, E.B. Hanlon, A. Marucci, P. Corio, S.D.M Brown, S.A. Empedocles, M.G. Bawendi, G. Dresselhaus, M.S. Dresselhaus, The anomalous

dispersion of the disorder-induced and the second-order Raman bands in carbon nanotubes, Brazilian Journal of Physics 30 (2000) 423-427.

[44] Y.C. Kimmel, D.V. Esposito, R.W. Birkmire, J.G. Chen, Effect of surface carbon on the hydrogen evolution reactivity of tungsten carbide (WC) and Pt-modified WC electrocatalysts, Int. J. Hydrogen Energy 37 (2012) 3019–3024.

Figure Captions

Fig. 1. SEM images of the initial precursor sample (a, b) and samples heated in helium atmosphere at 240 °C (c, d), 500 °C (e, f), 800 °C (g, h), 950 °C (i, j) and 1100 °C (k, l).

Fig. 2. X-ray diffraction patterns of the samples produced by heating of the precursor in helium atmosphere at 400 °C, 800 °C and 1100 °C (samples (I) and (III)).

Fig. 3. The WC:nC composite obtained by heating precursor (II) up to 1000 °C in helium atmosphere: (a) overview SEM image; (b) enlargement from area (1) showing tungsten carbide WC forming “chain” structures; (c) enlargement from area (2) showing WC nanoparticles in the carbon matrix; (d) - (f) high-resolution TEM images of WC tungsten carbide “chain” structures (the black arrows indicate the position of stacking faults, circles denote the positions from which fast Fourier transformation patterns were obtained).

Fig. 4. High-resolution TEM images of WC:nC composites obtained by heating precursor (II) up to 1000 °C in helium atmosphere: (a) bright field image TEM image showing WC nanoparticles and amorphous carbon; (b) high-angle annular dark field scanning transmission electron microscopy image with nanometre-sized WC particles in

an amorphous carbon matrix; (c) - (d) high-resolution episcopic microscopy image of multilayer carbon "onion" structures in the WC:nC composite, which have a spherical shape or the shape of multilayer tubes.

Fig. 5. SEM image of carbon produced as a result of the removal of WC from the WC:nC nanocomposite by means of acid treatment.

Fig. 6. Raman spectra of precursor (1) and samples produced by heating it at 400 °C (2) and 600 °C (3) in helium atmosphere.

Fig. 7. The Raman spectra of WC:nC (1) and carbon (2) produced by the removal of WC from the WC:nC nanocomposite by means of acid treatment.

Fig. 8. Overview spectrum of WC:nC powder recorded before Ar^+ beam etching (at the top) and the spectra of internal electronic states of W4f, C1s, and O1s before and after argon ion beam etching of the surface for 1, 4, and 14 min.

Fig. 9. Estimated content of W, C, and O atoms (at.%) in different chemical forms in the WC:nC powder. The data are given for the surface and for 1, 4, and 14 min of ion etching of the upper layers.

Tables

Table 1. Annealing temperature, composition, and morphology of precursor synthesis products.

Compound according to XPA data	**Temperature range, °C**	**Morphology according to microscopic analysis data**
$WO_2(C_3H_6O_3)$	200 – 240	Glassy mass
Amorphous phase	250 – 500	Formations including spheres with sphere

		diameter of 100-250 μm
$W_{18}O_{49}$	550 – 750	Spherical capsules to 100 μm in diameter filled with needles with ~20 nm cross-section and a length to 1500 nm
WO_2	750 – 800	Spherical capsules to 100 μm in diameter filled with rods with 300-500 nm cross-section and a length to 5000 nm
W	900 – 950	Aggregates of metallic tungsten in a carbon shell
W_2C	950 – 1000	Aggregates built of W_2C particles in a carbon shell
WC	1000 – 1100	Tungsten carbide particles with dimensions of the order of 50 nm

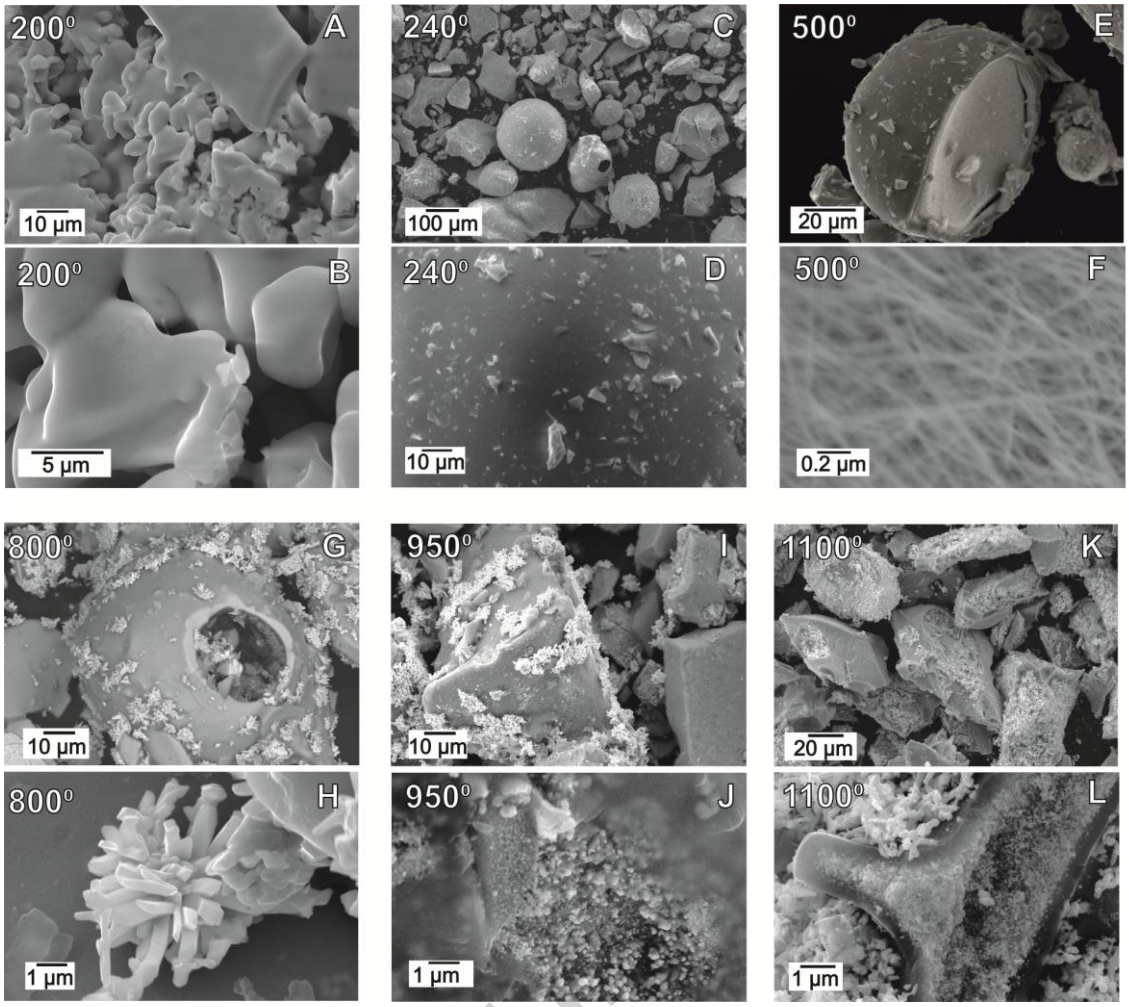
200⁰
A
10 µm
200⁰
B
5 µm
240⁰
C
100 µm
240⁰
D
10 µm
500⁰
E
20 µm
500⁰
F
0.2 µm
800⁰
G
10 µm
800⁰
H
1 µm
950⁰
I
10 µm
950⁰
J
1 µm
1100⁰
K
20 µm
1100⁰
L
1 µm

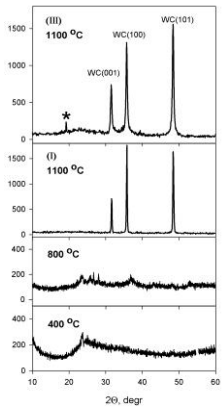
(III)
1100 °C
WC(101)
WC(100)
WC(001)
*
(I)
1100 °C
800 °C
400 °C
2θ, degr

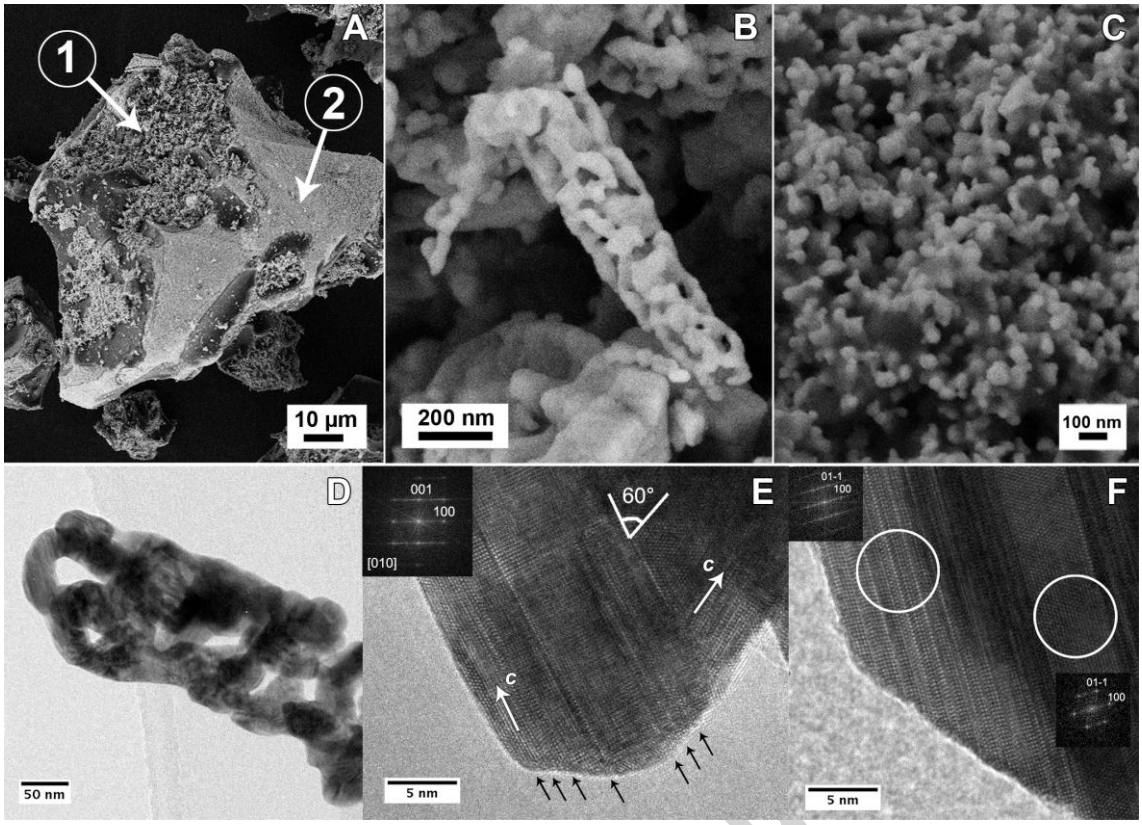

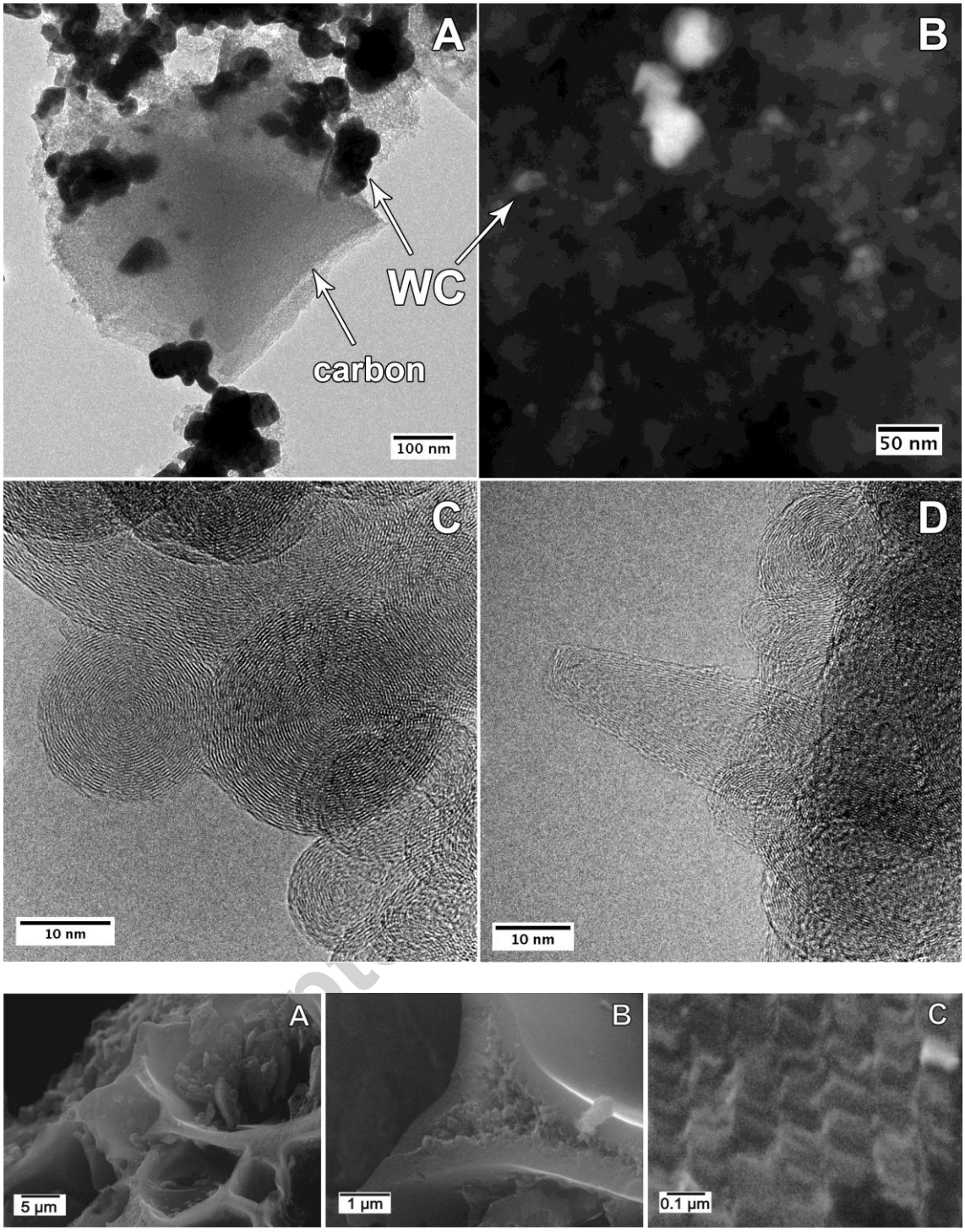
A
WC
carbon
100 nm
B
50 nm
C
10 nm
D
10 nm
A
5 µm
B
1 µm
C
0.1 µm

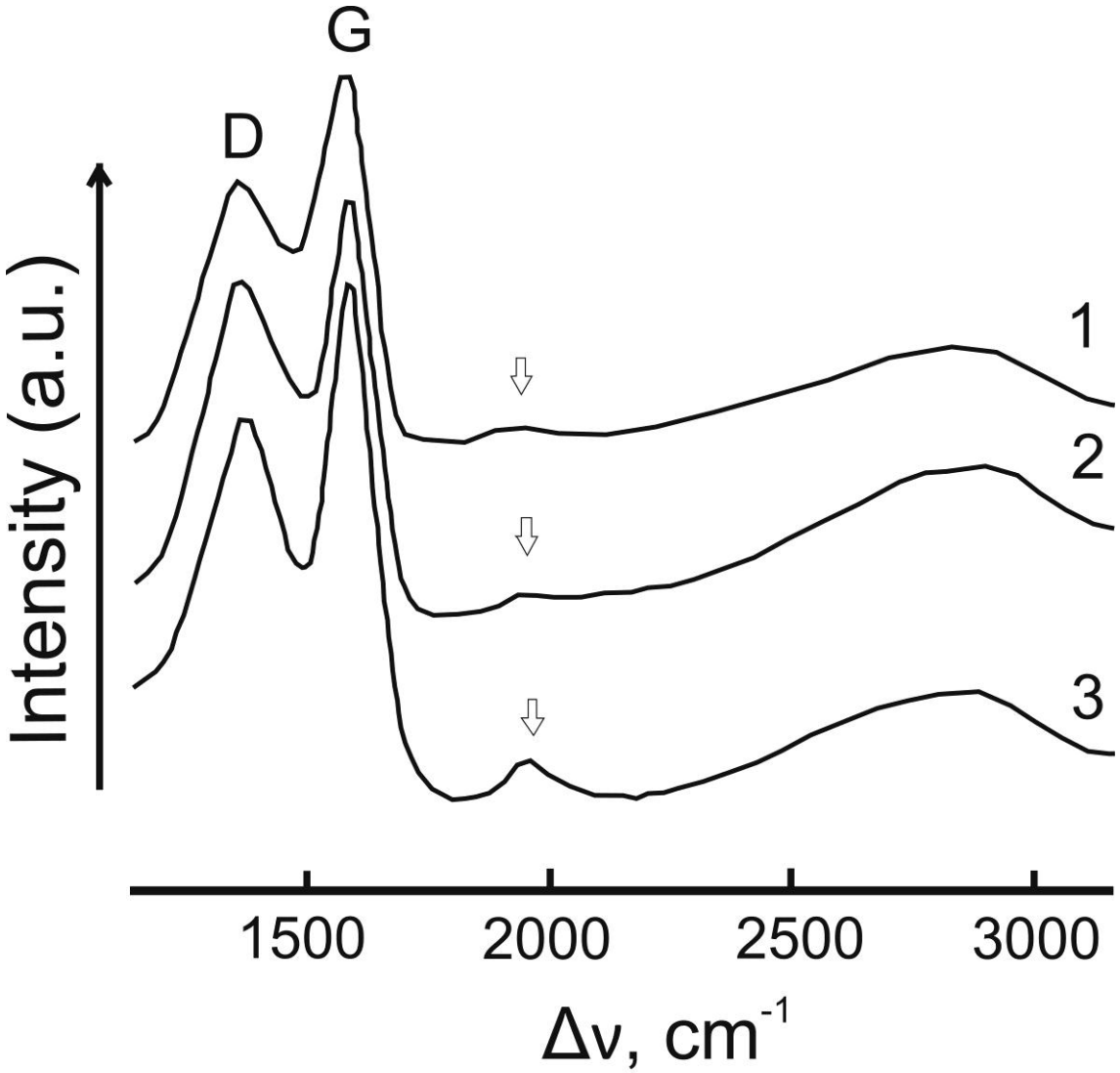

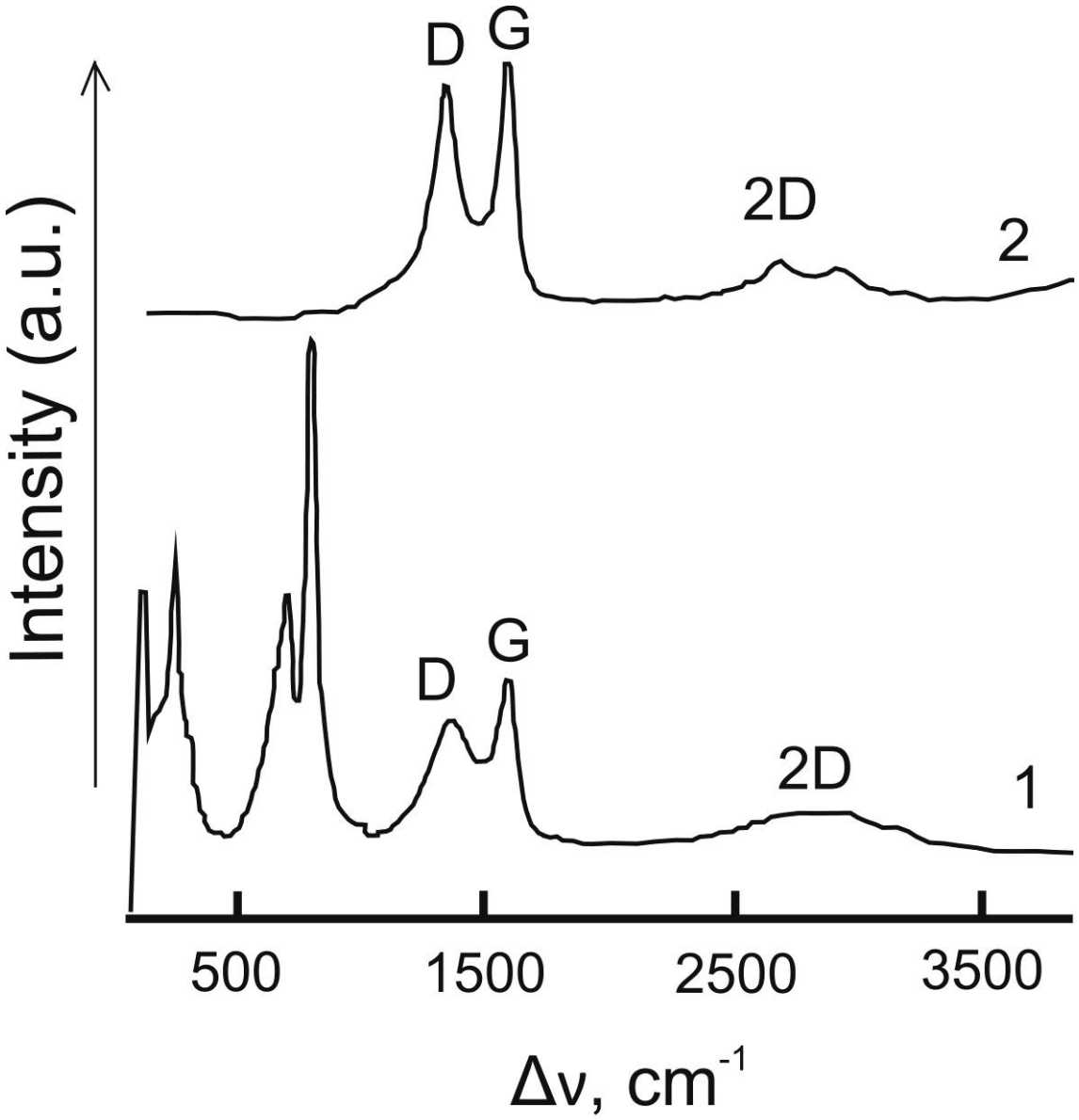

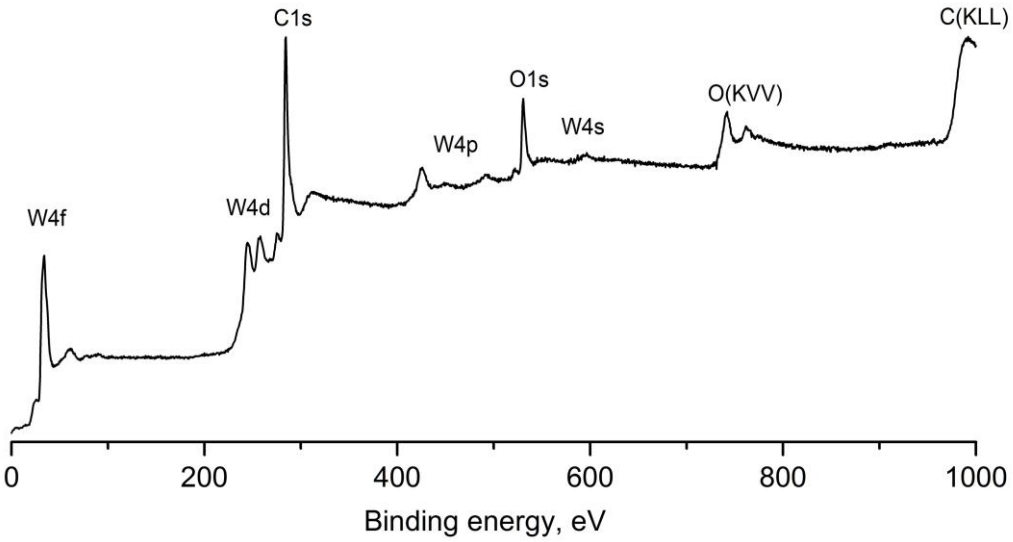
C1s
C(KLL)
O1s
O(KVV)
W4p
W4s
W4d
W4f
0
200
400
600
800
1000
Binding energy, eV

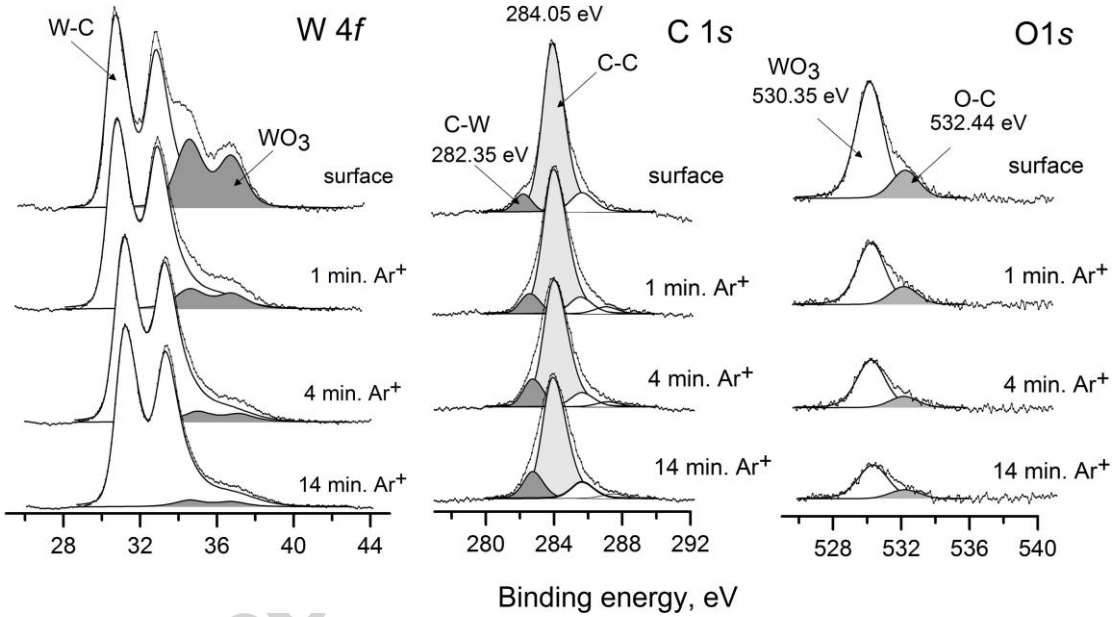
W-C
W 4f
WO3
surface
1 min. Ar+
4 min. Ar+
14 min. Ar+
28
32
36
40
44
284.05 eV
C 1s
C-C
C-W
282.35 eV
surface
1 min. Ar+
4 min. Ar+
14 min. Ar+
280
284
288
292
O1s
WO3
530.35 eV
O-C
532.44 eV
surface
1 min. Ar+
4 min. Ar+
14 min. Ar+
528
532
536
540
Binding energy, eV

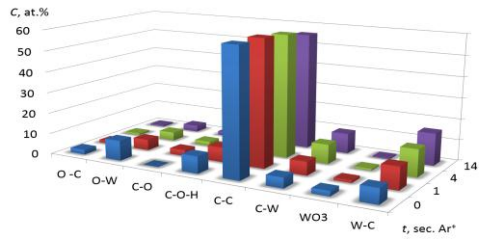
C, at.%
60
50
40
30
20
10
0
O -C
O-W
C-O
C-O-H
C-C
C-W
WO3
W-C
14
4
1
0
t, sec. Ar+